NEUROPHYSIOLOGY

Norepinephrine changes behavioral state through astroglial purinergic signaling

Alex B. Chen[1,2,3]*, Marc Duque[2,3], Altyn Rymbek[4], Mahalakshmi Dhanasekar[5], Vickie M. Wang[2,3], Xuelong Mi[6], Loeva Tocquer[5], Sujatha Narayan[1]†, Emmanuel Marquez Legorreta[1], Mark Eddison[1], Guoqiang Yu[7], Claire Wyart[5], David A. Prober[4], Florian Engert[2], Misha B. Ahrens[1]*

Both neurons and glia communicate through diffusible neuromodulators; however, how neuron-glial interactions in such neuromodulatory networks influence circuit computation and behavior is unclear. During futility-induced behavioral transitions in the larval zebrafish, the neuromodulator norepinephrine (NE) drives fast excitation and delayed inhibition of behavior and circuit activity. We found that astroglial purinergic signaling implements the inhibitory arm of this motif. In larval zebrafish, NE triggers astroglial release of adenosine triphosphate (ATP), extracellular conversion of ATP into adenosine, and behavioral suppression through activation of hindbrain neuronal adenosine receptors. Our results suggest a computational and behavioral role for an evolutionarily conserved astroglial purinergic signaling axis in NE-mediated behavioral and brain state transitions and position astroglia as important effectors in neuromodulatory signaling.

Neural circuits perform fast computations through precise patterns of synaptic connectivity and direct electrical coupling through gap junctions (*1*, *2*), but they can also be rapidly modulated by diffusible chemical messengers, including monoamines [such as norepinephrine (NE), dopamine, and serotonin] and neuropeptides (*3*–*5*). Such signaling accounts for a large portion of neural activity patterns that cannot be explained by synaptic connectivity alone (*6*–*8*) and has long been known to reconfigure synaptic networks to orchestrate behavioral states (*9*–*13*). Recent discoveries have shown that astroglia communicate bidirectionally with neurons through neuromodulatory signaling, suggesting that non-neuronal cells could play more important roles as neuromodulatory actuators than previously thought (*14*). Astrocytes and neurons have substantially different physiologies. Astrocytes are electrically inexcitable, exhibit local and global intracellular calcium transients, and have complex arbors of processes that form nonoverlapping territories and interact with thousands of individual neuronal synapses (*15*, *16*). However, how the specific physiology of astrocytes contributes to their role as active modulatory elements in neural circuits is still unresolved.

Our work focuses on three major neuromodulators, NE, adenosine triphosphate (ATP), and adenosine, and their role in mediating behavioral state changes. Since its discovery in the 1940s (*17*), NE has been known to profoundly influence neurophysiology, neural circuit dynamics, and behavior (*17*–*25*). Although the dominant assumption over the past eight decades has been that NE acts primarily through activation of adrenergic receptors on neurons, recent discoveries that NE also activates non-neuronal cells, particularly astroglia, challenge this assumption. In astroglia, NE triggers large intracellular calcium events caused by α1-adrenergic receptor (α1-AR) activation (*26*–*30*), but the specific roles played by astroglia in noradrenergic modulation remain unclear, as do the pathways linking NE-mediated astroglial calcium elevation to modulation of circuit activity.

As with NE, the purinergic signaling molecules ATP and adenosine are ubiquitous and critical neuromodulators. They play important roles in sleep-wake cycles (*31*–*33*), synaptic plasticity (*34*), and motor pattern generation (*35*), among other functions (*36*–*38*). Although astroglia have been argued to be a source of extracellular adenosine through ATP secretion (*34*, *36*) and extracellular ATP-to-adenosine metabolism (*39*), the behavioral relevance of such release remains, in many cases, controversial (*40*, *41*). Furthermore, whereas astroglial calcium elevation appears to trigger ATP secretion, the behavioral contexts that recruit astroglial purinergic signaling remain poorly understood because of the reliance on exogenous activation and/or ex vivo conditions in existing studies (*42*–*44*).

Leveraging the larval zebrafish, in which NE, ATP, and astroglial calcium can be imaged in conjunction with neural activity during behavior, we found that, during rapid behavioral state transitions, the noradrenergic and purinergic systems can be conceptualized as, respectively, fast excitatory and delayed inhibitory arms of a feedforward motif with astroglia as a coordinating intermediary. Therefore, beyond slow modulation of state, NE also acts through astroglial purinergic signaling to rapidly reconfigure circuit dynamics and enact behavioral state transitions.

NE neurons drive a biphasic futility response

Larval zebrafish have an innate tendency to stabilize their position by swimming in the direction of coherent visual flow (*45*, *46*). We have previously shown that when swims no longer move the fish forward, futility drives firing in hindbrain NE neurons, and NE signals through radial astroglia, a glial cell type similar to mammalian astrocytes (*47*, *48*), to suppress futile swims (*49*). Here, we made use of our previously published behavioral assay for futility-induced passivity in larval zebrafish (*49*, *50*). Fish were immobilized in agarose and their tails freed. The animals' tail positions were then automatically tracked, and detected swims were used to deliver realistic online visual feedback through projection of drifting grating stimuli to the floor of the chamber (Fig. 1A and materials and methods). To encourage robust swimming behavior, we delivered a steady, constant-velocity forward drifting grating (*45*) (Fig. 1B). Simultaneously, we manipulated the efficacy of the fish's swims by cycling between two stimulus conditions: closed loop and open loop. During closed loop, the fish's swim attempts resulted in visual feedback (backward drift of the visual stimuli) to signal successful forward swimming (Fig. 1B, left). In open loop, swim attempts resulted in no change to the visual stimulus (Fig. 1B, right) and were thus futile. Futility is encoded by a population of NE neurons in the medulla oblongata known as NE-MO neurons [putatively homologous to mammalian cluster A2 (*51*)], and NE-MO activation drives astroglial calcium elevation to drive motor-inhibitory GABAergic neurons in the lateral medulla oblongata (L-MO) (Fig. 1C) (*49*).

Consistent with previous work (*26*, *49*), we found that behavioral futility signaled by a lack of visual feedback caused fish to enter, with a delay, a passive state, in which swimming ceases for tens of seconds (Fig. 1, D and E; fig. S1; and movie S1). Before passivity, fish exhibited an increase in swim vigor and were more likely to perform high-amplitude, struggle-like swims (Fig. 1, D and E, and fig. S1). Although NE-MO activation was previously shown to cause passivity (*49*), the contribution of NE neurons in the transient up-regulation of swim vigor at futility onset has not been thoroughly investigated. Given NE's well-documented ability to

[1]Janelia Research Campus, Howard Hughes Medical Institute, Ashburn, VA, USA. [2]Department of Molecular and Cellular Biology, Harvard University, Cambridge, MA, USA. [3]Graduate Program in Neuroscience, Harvard Medical School, Boston, MA, USA. [4]Tianqiao and Chrissy Chen Institute for Neuroscience, Division of Biology and Biological Engineering, California Institute of Technology, Pasadena, CA, USA. [5]Sorbonne Université, Paris Brain Institute (Institut du Cerveau, ICM), Institut National de la Santé et de la Recherche Médicale U1127, Centre National de la Recherche Scientifique Unité Mixte de Recherche 7225, Assistance Publique–Hôpitaux de Paris, Campus Hospitalier Pitié-Salpêtrière, Paris, France. [6]Bradley Department of Electrical and Computer Engineering, Virginia Polytechnic Institute and State University, Arlington, VA, USA. [7]Department of Automation, Tsinghua University, Beijing, P.R. China. †Present address: Allen Institute for Brain Science, Seattle, WA, USA. ***Corresponding author. Email: abchen@g.harvard.edu (A.B.C.); ahrensm@janelia.hhmi.org (M.B.A.)**

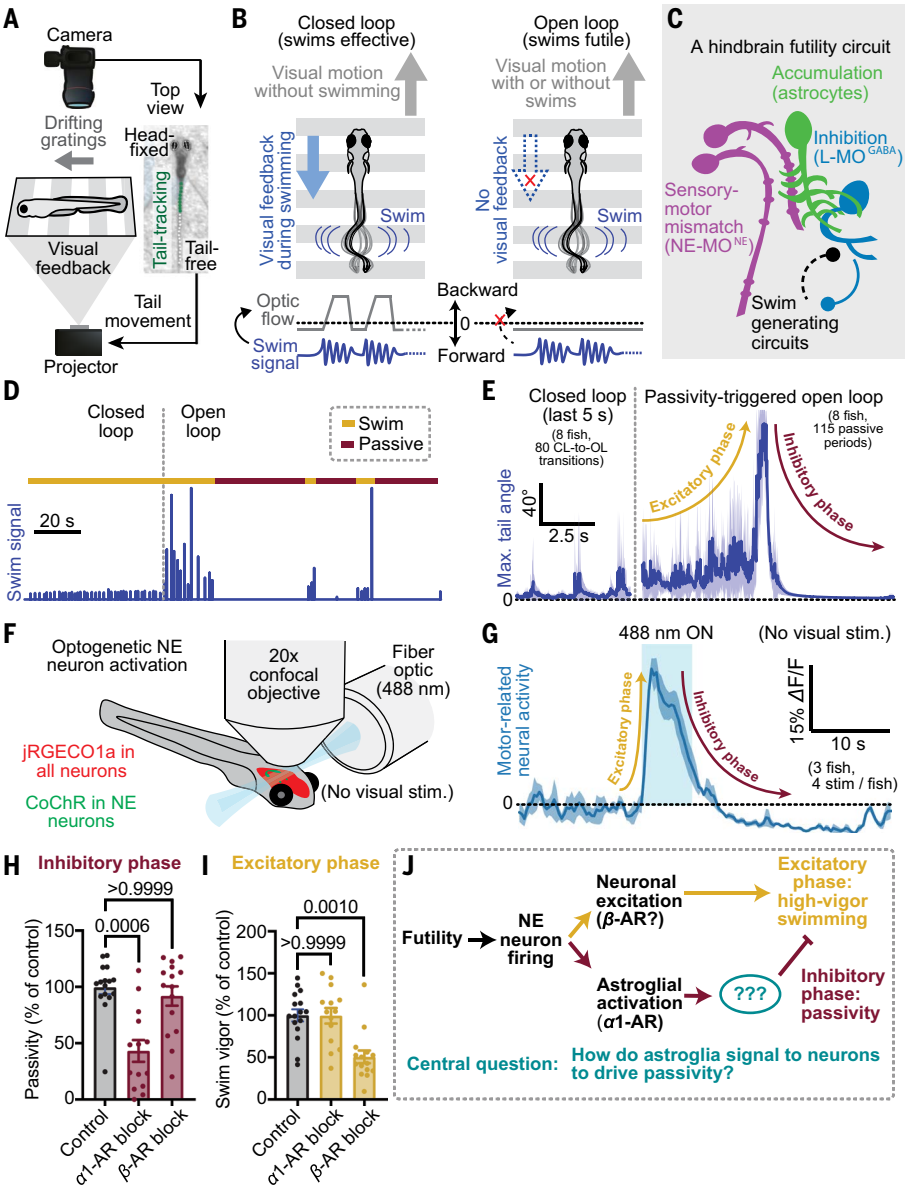

Fig. 1. Futility triggers a biphasic behavioral and neural response through NE neuron activation. (**A**) Schematic of virtual reality behavioral experiments with real-time swim detection and visual feedback. (**B**) Diagram illustrating the difference between closed-loop (visual feedback in response to swims) and open-loop (no visual feedback) conditions. (**C**) Schematic of the known cell types involved in futility-induced passivity. (**D**) Swim trace of an example trial demonstrating closed-loop and open-loop swim behavior. (**E**) Average closed-loop and passivity-triggered open-loop tail angle demonstrating an initial increase in swim amplitude (excitatory phase) followed by inhibition of swimming (inhibitory phase) in open loop. (**F**) Neural activity imaged with a confocal microscope while NE neurons were optogenetically activated using a fiber-optic cable. (**G**) Optogenetic stimulation–triggered average of neural activity in motor areas demonstrating fast excitation and delayed inhibition, similar to the behavioral futility response. (**H** and **I**) Effect of blocking α1-ARs (with 100 μM prazosin) or β-ARs (with 100 μM propranolol) on open-loop passivity (H) and open-loop swim vigor (I). For (H) and (I), $n = 16$ control, $n = 14$ α1-AR block, and $n = 15$ β-AR block fish. For (H), $P > 0.9999$ for control versus β-AR block fish and $P = 0.0006$ for control versus α1-AR block fish. For (I), $P = 0.001$ for control versus β-AR block fish and $P > 0.9999$ for control versus α1-AR block fish by Kruskal-Wallis test. (**J**) Model of parallel noradrenergic channels that contribute to the excitatory and inhibitory phases of the futility response and central problem statement. All error bars and shaded error regions represent SEM.

enhance arousal and effort (*21*, *52*), we tested whether NE neuron firing immediately promotes the rapid enhancement of vigor, in addition to driving temporally delayed swim inhibition (Fig. 1F and fig. S2). We found that optogenetic stimulation of NE neurons drove fast excitation and persistent but delayed inhibition of hindbrain motor circuits (Fig. 1G and fig. S2, A to C). We further observed that persistent inhibition of motor circuits coincided with sustained activity in L-MO (*49*) (fig. S2D). Therefore, in larval zebrafish, behavioral futility promotes a biphasic response in both behavior and neural dynamics, which can be defined as an excitatory phase consisting of increased behavioral vigor, followed by an inhibitory phase involving behavioral suppression (Fig. 1, E and G). Both phases are driven by NE neuron firing.

NE neurons act on downstream targets through activation of α-ARs and β-ARs by NE, as well as through fast synaptic excitation through co-released glutamate. Astroglial calcium elevation through α1-AR activation has been shown to be both necessary and sufficient for the inhibitory phase of the futility response in larval zebrafish (*49*), but its relationship to the excitatory phase of the futility response is less understood. Our findings suggest that astroglial calcium signaling is not involved in the excitatory phase. First, optogenetic stimulation of NE neurons elevated astroglial calcium with a temporal delay likely too long to account for the more rapid increase in motor activity (fig. S3A). Second, inhibition of α1-AR signaling with prazosin, which completely abolishes NE-evoked astroglial calcium responses (*49*), had no effect on futility-induced vigor enhancement but did suppress futility-induced passivity (Fig. 1, H and I). Thus, α1-AR signaling and astroglial calcium elevation are likely dispensable for the excitatory phase.

The activation of α1-ARs and downstream astroglial calcium elevation seem to act in a feedforward inhibitory–like manner. Feedforward inhibition in synaptic networks serves to sharpen the window of excitatory drive (*53*, *54*). Similarly, elevating astroglial calcium activation through optogenetic stimulation in *Tg(gfap:CoChR-eGFP)* fish or inhibiting calcium using prazosin shortened or lengthened the window of higher-vigor open loop swimming, respectively (fig. S3, B and C). Furthermore, longer-duration NE-MO stimulation reliably triggered swim cessation within a few seconds (fig. S3D) despite NE likely remaining elevated for much longer (*50*). This is consistent with feedforward inhibition, rather than feedback inhibition, of noradrenergic drive.

Conversely, blockade of β-ARs strongly attenuated the excitatory phase (Fig. 1, H and I), suggesting that different adrenergic receptor subtypes may implement different aspects of the futility response. Blocking β-ARs also reduced passivity in some fish, potentially because inhibiting the excitatory phase reduces higher-vigor struggles, leading to less NE release (*26*, *49*) and lowering subsequent passivity. Alternatively, β-ARs could mediate feedback inhibition of the excitatory phase. In any case, specific astroglial involvement in the inhibitory phase raises a fundamental question that is central to this work (Fig. 1J): Because neurons ultimately control motor output, how do astroglia signal to downstream neurons to drive the inhibitory phase by suppressing swimming?

Futility-induced, NE-dependent astroglial ATP release

We reasoned that astroglia likely communicate with downstream neurons by secreting a neuroactive substance. In particular, we hypothesized that futility drives calcium-dependent astroglial release of ATP, because glial-derived ATP can modulate neural activity in other contexts (*43*, *44*, *55*, *56*). To investigate whether futility-induced astroglial calcium elevation leads to release of ATP, we generated a fish line (*Tg(gfap:GRAB$_{ATP}$;gfap:jRGECO1a)*) expressing GRAB$_{ATP}$, an extracellular green fluorescent ATP sensor (*57*), as well as the intracellular red fluorescent calcium sensor jREGCO1, in astroglia (see the materials and methods). First, we validated the specificity of GRAB$_{ATP}$ for ATP over adenosine in fish (fig. S4A). We then performed simultaneous brain-wide functional imaging of both glial calcium and secreted ATP while immobilized animals behaved in virtual reality (see the materials and methods) (Fig. 2A). We found that during open-loop swimming, both astroglial intracellular calcium and extracellular ATP around astroglia exhibited a rapid elevation throughout the hindbrain, followed by a slower return to baseline over tens of seconds (Fig. 2, B to D).

These data suggest that astroglia, and not neurons, release ATP during futile swimming. However, because the ATP sensor used is extracellular, it cannot distinguish between astroglial-secreted ATP and ATP released by neurons near astroglial processes. However, five additional lines of evidence support an astroglial origin for the released ATP. First, ATP elevation lags behind intracellular astroglial calcium elevation (fig. S4, B to D), consistent with astroglial calcium elevation causing ATP release. Second, simultaneous imaging of neuronal calcium activity and extracellular ATP revealed that neuronal calcium elevation failed to reliably predict ATP release, whereas glial calcium events were always accompanied by ATP elevation (fig. S4, E to G). Third, inhibition of astroglial calcium with pharmacological blockade of α1-ARs strongly attenuated both futility-triggered ATP elevation (Fig. 2E) and astroglial calcium (fig. S4H), but had no effect on closed-loop ATP or astroglial calcium dynamics (fig. S4H). Because this pharmacological manipulation is not cell-type specific we also generated a fish expressing the calcium extruder hPMCA2 specifically in astroglia (*Tg(gfap:hPMCA2-mCherry)*). Astroglial-specific hPMCA2 expression

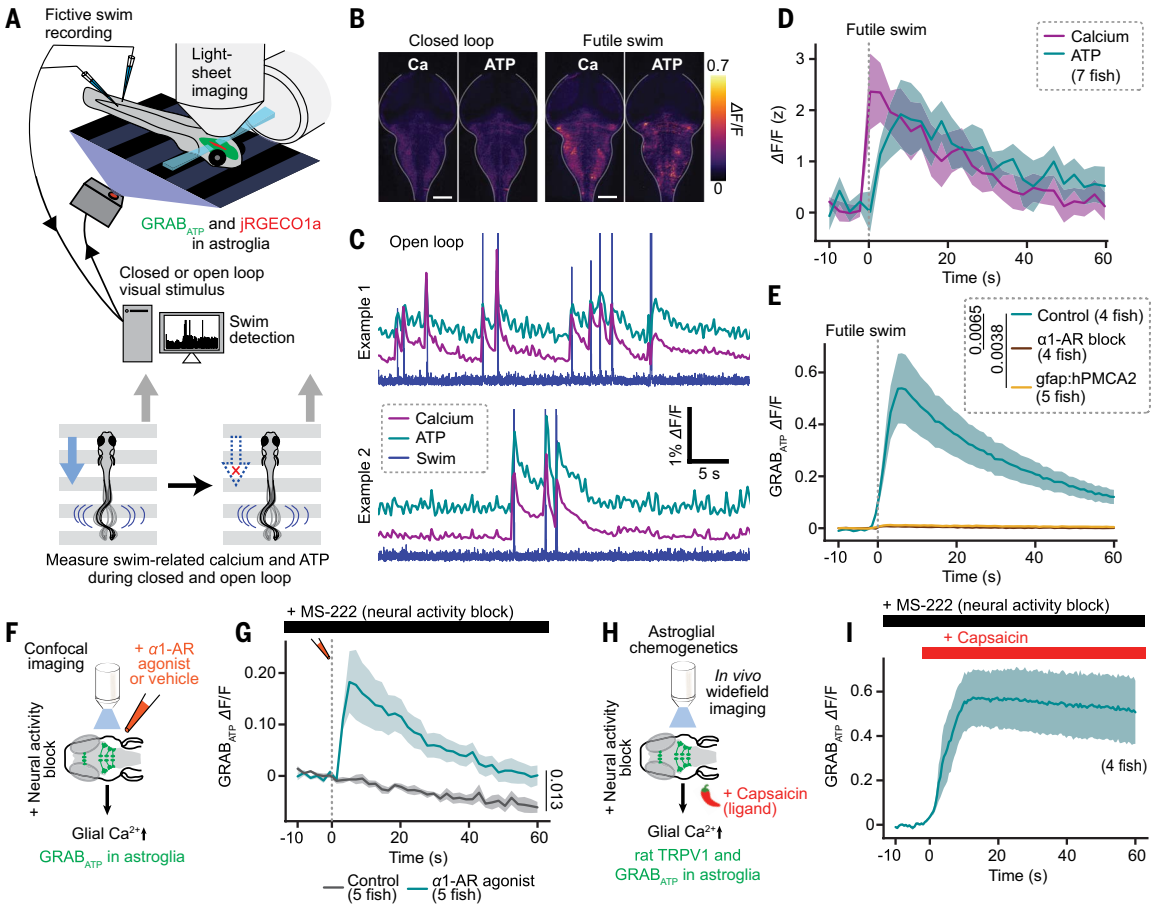

Fig. 2. Futility drives astroglial release of ATP. (**A**) Experimental schematic: two-color light-sheet imaging of extracellular ATP and astroglial calcium in *Tg(gfap:GRAB$_{ATP}$;gfap:jRGECO1a)* fish along with fictive behavioral recording. (**B**) Fluorescence micrographs of simultaneously collected GRAB$_{ATP}$ and jRGECO1a signals in a fish in baseline condition or during a futile swim. (**C**) Two examples of motor nerve electrical activity, GRAB$_{ATP}$ and jRGECO1a, signals during open-loop periods. Swim, calcium, and ATP traces are manually offset along the vertical axis to allow for better visualization. (**D**) Futile swim–triggered astroglial calcium and extracellular ATP signals averaged across fish ($n = 7$). (**E**) Futile swim–triggered GRAB$_{ATP}$ signal in fish treated with an α1-AR blocker (100 μM prazosin) or vehicle and in fish expressing hPMCA2 in astroglia ($n = 4$ control, $n = 5$ α1-AR block, and $n = 5$ hPMCA2). $P = 0.0065$ for control versus α1-AR block fish and $P = 0.0038$ for control versus hPMCA2 fish. Kruskal-Wallis test on area under the curve (AUC) from 0 to 60 s was used. (**F**) Experimental schematic: ex vivo confocal imaging during puffing of an α1-AR agonist (10 μM methoxamine) or vehicle in the presence of a neural activity blocker (160 mg/liter MS-222, a sodium channel inhibitor) in *Tg(gfap:GRAB$_{ATP}$)* fish. (**G**) GRAB$_{ATP}$ signal in fish in experiments described in (F) triggered on puff and futility onset aligned ($n = 5$ for both conditions). $P = 0.013$, Mann-Whitney on AUC from 0 to 60 s. (**H**) Experimental schematic: in vivo wide-field imaging during chemogenetic activation of *Tg(gfap:rTRPV1-eGFP)* fish with 200 nM capsaicin in the presence of a neural activity blocker (170 mg/L MS-222). (**I**) GRAB$_{ATP}$ signal in fish treated with capsaicin as described in (F) triggered capsaicin administration and futility onset aligned. All error bars and shaded error regions represent SEM.

inhibited astroglial calcium elevation during futile swims (fig. S5A) and, accordingly, decreased the duration of passivity in open loop (fig. S5, B to E). This effect was not caused by a decrease in general health of the animal or in the health of astroglia, because animals expressing hPMCA2 in astroglia behaved similarly to their wild-type siblings during normal swimming (fig. S5, F to H) and had astroglia that still exhibited microdomain calcium events (fig. S5, I to K). Inhibiting glial calcium elevation with hPMCA2 also suppressed futile swim–evoked ATP elevation (Fig. 2E). Fourth, pharmacological activation of α1-ARs was sufficient to cause ATP elevation even when neural activity was inhibited with a sodium channel blocker (Fig. 2, F and G). Finally, direct chemogenetic activation of astroglia also elevated ATP when neural activity was inhibited (Fig. 2, H and I). Neither pharmacological nor chemogenetic astroglial activation affected neuronal activity under conditions of sodium channel block (fig. S6, A and B). These converging lines of evidence implicate NE-mediated astroglial, and not neuronal, calcium signaling as being critical for extracellular ATP elevation during behavioral futility.

ATP promotes passivity through extracellular metabolism into adenosine

We investigated whether ATP elevation promotes passivity by treating fish with NPE-caged ATP, a P(3)-[1-(2-nitrophenyl)]ethyl ester of ATP that is pharmacologically inert until exposed to ultraviolet (UV) light (Fig. 3A). Freely swimming fish treated with caged ATP or vehicle were exposed to UV light, and passivity duration was recorded. UV light constitutes an inescapable aversive stimulus, conceptually similar to the open-loop conditions described in Fig. 1. As a result, fish exposed to UV light eventually exhibited futility-induced passivity after a period of high-vigor swimming (Fig. 3B and fig. S7A). However, fish treated with caged ATP exhibited increased passivity compared with vehicle controls (Fig. 3, B and C) while exhibiting no difference in struggle onset or time to peak swimming (fig. S7B). Therefore, ATP elevation drives the inhibitory, but not the excitatory, phase of futility-induced passivity.

Having established that ATP is an astroglia-to-neuron signal that induces passivity, we next sought to determine the mechanism through which ATP release suppresses swimming. ATP directly binds to two families of purinergic (P2) receptors, ionotropic P2X receptors and metabotropic P2Y receptors. Broad P2 receptor inhibition with suramin (100 μM bath administration) did not inhibit futility-induced passivity (Fig. 3D). This result suggests that although ATP elevation drives passivity, P2 purinergic receptors do not mediate futility-induced swimming suppression.

Because direct action of ATP does not seem to play an important role in futility-induced passivity, we considered an alternative hypothesis in which the ATP metabolite adenosine acts directly on neurons and suppresses swimming. Once secreted into the extracellular space, ATP is rapidly metabolized into adenosine through the action of two membrane-localized, extracellular-facing enzymes: Cd39 (or Entpd), which converts ATP into AMP by hydrolyzing the γ- and β-phosphate residues of ATP, and Cd73 (or Nt5e), which catabolizes AMP into adenosine (*39*) (Fig. 3E). In the spinal cord, such extracellular ATP-to-adenosine conversion is thought to contribute to locomotor rhythms (*35*). We performed two experiments to test the involvement of both components of this extracellular, biochemical pathway in futility-induced passivity. First, we blocked Cd73 with AMPCP and found that futility-induced passivity was inhibited (Fig. 3, E and F). Additionally, we treated fish with ARL 67156, a nonhydrolyzable ATP analog and competitive Cd39 inhibitor (Fig. 3E), and used optogenetics to directly activate astroglia (fig. S7C). Consistent with our previous work (*49*), optogenetic stimulation of astroglia caused passivity in untreated fish, mimicking the effect of astroglial calcium increases during natural futility-induced passivity. However, pretreatment with ARL 67156 delayed passivity in response to optogenetic astroglial stimulation (Fig. 3G). Although optogenetic stimulation of astroglia has been shown in some cases to elicit nonphysiological calcium responses (*58*–*60*), the stimulation here elicited behavioral output similar to open-loop visual stimuli. These results indicate that the passivity-stimulating action of extracellular ATP is mediated by extracellular biochemical pathways that metabolize it into adenosine.

To directly visualize extracellular adenosine dynamics during futility-induced passivity, we generated a fish line expressing the extracellular green fluorescent adenosine sensor $GRAB_{Ado1.0}$ (*32*) in neurons and found that, as predicted by our behavioral experiments (Fig. 3, E to G), extracellular adenosine increased during futile swims (Fig. 3, H and I). Preventing astroglial activation, and therefore ATP release, by blocking α1-ARs with prazosin abolished futility-induced adenosine elevation (Fig. 3I, blue). Further, inhibiting metabolism of astroglial-secreted ATP into adenosine with ARL 67156 attenuated adenosine buildup during futility (Fig. 3I, red). Finally, inhibiting ATP-to-adenosine metabolism prevented $GRAB_{Ado1.0}$ elevation to exogenously applied ATP (fig. S8, A and B). These experiments indicate that adenosine elevation, downstream of astroglial ATP release, is a component of the futility-induced astroglial noradrenergic-to-purinergic pathway.

Adenosine acts as a signaling molecule in the central nervous system primarily by binding G protein–coupled adenosine receptors. To assess the involvement of adenosine receptors in the futility response, we performed pharmacological experiments to either drive or inhibit adenosine receptor signaling. We found that the adenosine receptor agonist 2-chloroadenosine increased passivity and decreased the swim rate in both closed loop and open loop (fig. S8, C to E), demonstrating that adenosine receptor activation is sufficient to trigger passivity. Nonspecific inhibition of adenosine receptor signaling with caffeine, an adenosine receptor antagonist, suppressed open-loop passivity (Fig. 3J, left) but had no effect on open-loop struggle probability (Fig. 3J, right). The suppression of passivity did not result from effects upstream of astroglial calcium, because caffeine did not decrease astroglial calcium elevation or ATP secretion in response to NE (if anything, both seemed to increase after caffeine treatment, but the effect was variable) (fig. S8, F and G). Caffeine has off-target effects unrelated to its inhibition of adenosine receptors. However, we found that directly buffering adenosine with the high-affinity sensor $GRAB_{Ado1.0}$ also resulted in a small but significant reduction in futility-induced passivity compared with their wild-type siblings (fig. S8H, $P = 0.0355$). Finally, more specific blockade of A2B adenosine receptors (A2BRs), but not A1Rs or A2ARs, inhibited futility-induced passivity (Fig. 3, K and L). Therefore, the astroglial noradrenergic-to-purinergic pathway recruited by futility implements the inhibitory, but not excitatory, phase of the futility response primarily through A2Rs on downstream neurons.

Adenosine drives swim-suppressing neurons in the lateral medulla

Neurons are the cells that ultimately control swimming. Therefore, we reasoned that futility-induced astroglial adenosine release acts on neural targets to drive passivity. Because our pharmacological evidence supported a role for the A2BR (Fig. 3L), we performed in situ hybridization with probes targeting *adora2b* (mRNA for A2BR) transcripts and found, consistent with previous reports (*61*), *adora2b* expression in the midbrain and hindbrain, near the midline and in the subventricular zone (SVZ), as well as in bilaterally symmetrical hindbrain neuronal populations (fig. S9). Neuronal expression of *adora2b* appeared anatomically proximal to L-MO, a population that is activated by futility and suppresses swimming (Fig. 4, A and B, and fig. S10) (*49*). Imaging L-MO activity during behavior in *Tg(elavl3:jRGECO1a)* fish revealed that inhibition of adenosine receptors with caffeine reduced the magnitude and duration of persistent L-MO activation triggered by high-amplitude futile swims (Fig. 4C). This reduction was also reflected in a decrease in average futility-triggered passivity duration (Fig. 4D). Possible interpretations of the remaining struggle-induced L-MO activation is an incomplete block by caffeine or occurring through mechanisms independent of adenosine receptor activation. Furthermore, chemogenetic activation of astroglia using *Tg(gfap:TRPV1-eGFP;elavl3:jRGECO1a)* fish increased the rate of L-MO activation events, and the adenosine receptor

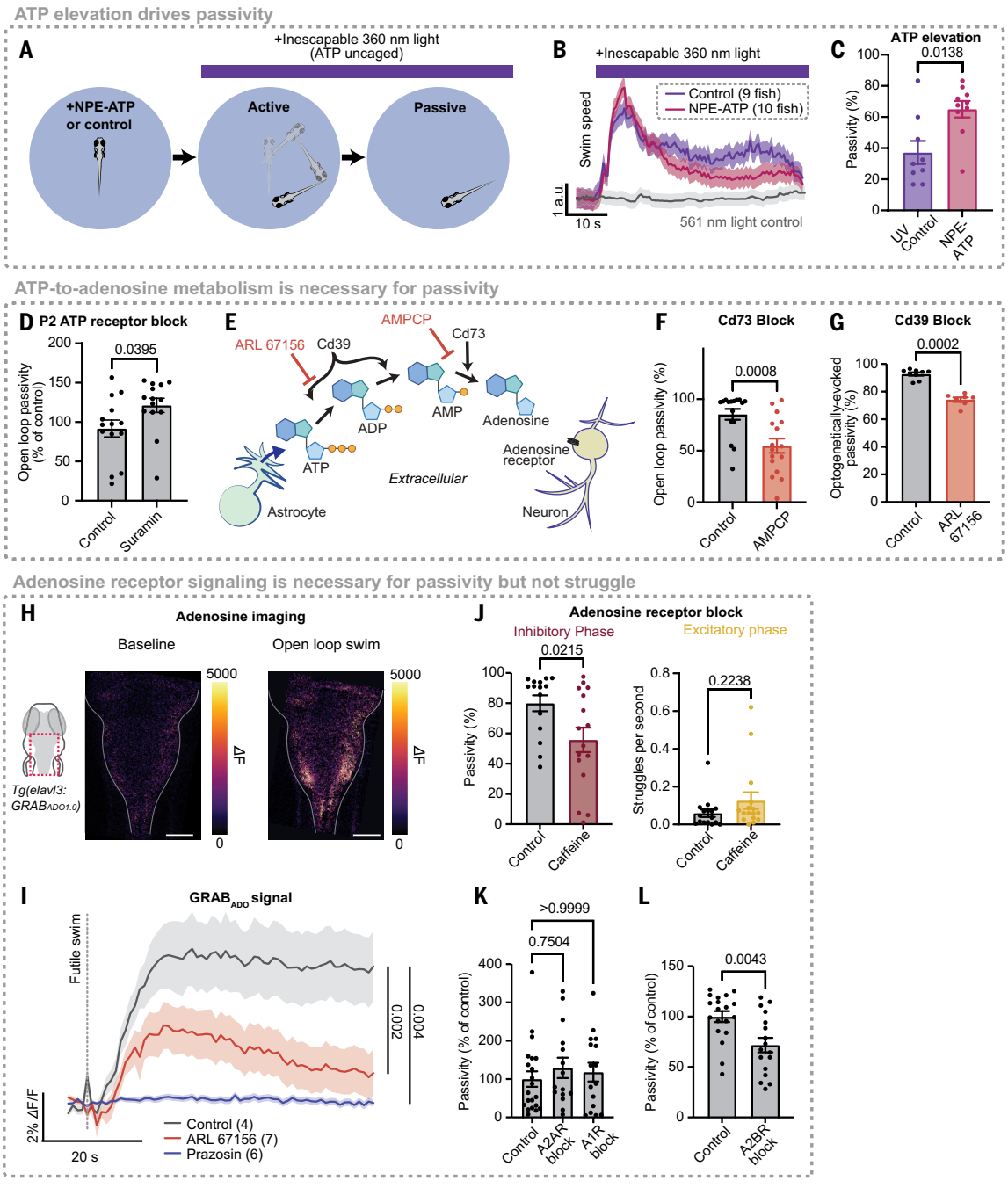

Fig. 3. ATP promotes passivity through extracellular metabolism into adenosine. (**A**) Experimental schematic: behavioral recording of freely swimming fish treated with 100 μM NPE-ATP or vehicle and then subjected to inescapable UV (360 nm) light, which uncages ATP. (**B**) Light onset–triggered swim speed of fish treated with NPE-ATP or vehicle. (**C**) Percentage of light ON period spent passive for vehicle control and NPE-ATP–treated fish ($n = 9$ control and $n = 10$ NPE-ATP fish). $P = 0.0138$, Mann-Whitney test. (**D**) Effect of a P2 receptor blocker (100 μM suramin) or vehicle on open-loop passivity in head-fixed behavior ($n = 14$ control and $n = 14$ suramin-treated fish). $P = 0.0395$, Mann-Whitney test. (**E**) Diagram illustrating the extracellular biochemical ATP-to-adenosine pathway through the enzymes Cd39 and Cd73 and pathway inhibition by the competitive Cd39 inhibitor ARL 67156 and the Cd73 inhibitor AMPCP. (**F**) Effect of Cd73 block (100 μM AMPCP) on open-loop passivity in head-fixed behavior ($n = 16$ control and $n = 16$ AMPCP fish). $P = 0.0008$, Mann-Whitney test. (**G**) Percentage passivity after the onset of optogenetic stimulation for fish treated with ARL 67156 or vehicle ($n = 9$ control and $n = 7$ ARL 67156 fish). $P = 0.0002$, Mann-Whitney test. (**H**) Extracellular adenosine ($GRAB_{ADO1.0}$) signal of a fish in baseline (left) and during a futile swim (right). (**I**) Futile swim–triggered average of $GRAB_{ADO1.0}$ signal in fish treated with vehicle, an α1-AR blocker (100 μM prazosin), or a Cd39 inhibitor (1 mM ARL 67156) ($n = 4$ control, $n = 7$ ARL 67156, and $n = 6$ prazosin fish). $P = 0.002$ for control versus ARL and $P = 0.004$ for control versus prazosin, Kruskal-Wallis on AUC from 0 to 60 s after futile swim. (**J**) Effect of vehicle or adenosine receptor blocker (100 μM caffeine) on the proportion of open loop spent passive (left) and open-loop struggle rate (right) ($n = 15$ control and $n = 16$ caffeine). $P = 0.0215$ for proportion passivity and $P = 0.2238$ for struggle rate, Mann-Whitney test. (**K** and **L**) Effect of an A1R blocker (DPCPX) and an A2AR blocker (SCH-58261) (K) or an A2BR blocker (MRS 1754) (L) on proportion of open loop spent passive. For (K), $n = 21$ control, $n = 15$ DPCPX and $n = 16$ SCH-58261. For (L), $n = 19$ control and $n = 17$ MRS 1754. All error bars and shaded error regions represent SEM.

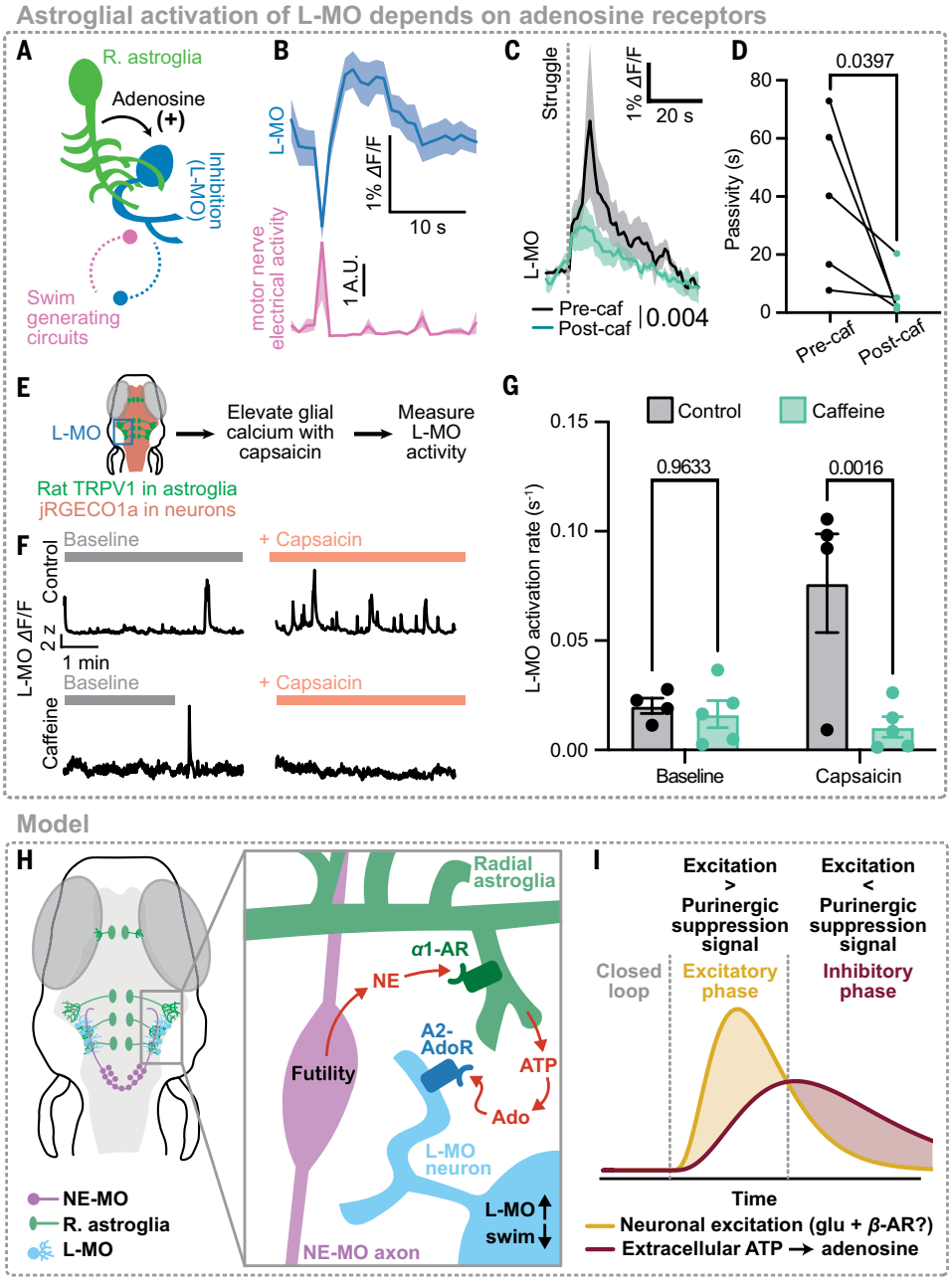

Fig. 4. Adenosine persistently activates the swim-suppressing region L-MO. (**A**) Schematic: astroglial communication with L-MO and mutual inhibition between L-MO and motor regions. (**B**) Example of L-MO neuronal activity anticorrelation to swim vigor in one fish. (**C**) Struggle-evoked L-MO activity before and after caffeine (100 μM). Shown is the mean across five fish ($n = 5$). $P = 0.004$, Mann-Whitney on AUC from 0 to 60 s after struggle. (**D**) Mean of futility swim–triggered passivity durations before and after caffeine treatment ($n = 5$). $P = 0.0397$, paired t test. (**E**) Schematic: activating astroglia in *Tg(gfap:TRPV1-eGFP;elavl3:JRGECO1a)* fish while imaging L-MO activity using light-sheet microscopy. (**F**) L-MO activity in four example fish treated with either vehicle control (top row) or 100 μM caffeine (an adenosine receptor blocker, bottom row) or vehicle control, either in baseline untreated condition (left) or with capsaicin (right). (**G**) Summary of rate of L-MO activation across all fish and conditions ($n = 4$ control and $n = 5$ caffeine). $P = 0.9633$ for baseline control versus caffeine and $P = 0.0016$ for capsaicin control versus caffeine, two-way ANOVA with Šídák's multiple-comparisons test. (**H**) Model: futility-triggered NE release drives astroglial ATP release. ATP is metabolized extracellularly into adenosine, and adenosine activates A2 adenosine receptors in L-MO to increase L-MO activity and suppress swimming. (**I**) Model: futility-related NE-MO firing drives fast excitation (yellow). NE mediates delayed inhibition (red) through astroglial activation, ATP release, and ATP-to-adenosine metabolism. Eventually, inhibition overcomes fast excitation to drive the inhibitory phase of passivity. Thus, an astroglial noradrenergic-to-purinergic pathway mediates feedforward inhibition of the passivity response. All error bars and shaded error regions represent SEM.

antagonist caffeine inhibited this increase but had no effect on baseline L-MO activity (Fig. 4, E to G). A caveat of this experiment is that our chemogenetic activation of astroglia causes astroglial calcium elevation across large areas of the brain; therefore, in this experiment we cannot rule out involvement of regions beyond L-MO in suppressing swimming. However, we previously demonstrated that L-MO is likely the primary driver of futility-induced passivity (*49*). Altogether, these data provide evidence that the purinergic signal released by astroglia exerts feedforward inhibition on motor circuits through the activation of inhibitory neurons in L-MO through A2BRs (Fig. 4, H and I).

Discussion

Our work shows that the rapid state transition orchestrated by NE proceeds through astroglia using purinergic neuromodulation. We identified a functional logic connecting these two critical neuromodulatory systems: Noradrenergic neurons drive fast excitation but also recruit purinergic signaling through astroglia to implement delayed, feedforward inhibition. Thus, astroglia play a central role in coordinating across different neuromodulatory systems.

The NE-astroglia-purinergic pathway is recruited when actions become futile and a behavioral state change is necessary, analogous to NE-mediated transitions under the "global model failure" conceptualization of NE function (*18*–*20*, *62*). The components of this pathway, monoamine-triggered astroglial calcium signaling, astroglial ATP release, extracellular ATP-to-adenosine conversion, and adenosinergic suppression of neural activity, are ubiquitous across brain regions and species, which suggests that this conserved NE-astroglia-purinergic (NAP) signaling motif could be a fundamental computational unit implementing feedforward inhibition over neuromodulatory timescales (*63*–*65*). Indeed, a companion paper by Lefton *et al.* (*66*) demonstrates that NE's well-known depressive effect on excitatory synapses in mice proceeds entirely through this same NE-astroglia-ATP/adenosine pathway, and several additional emerging lines of evidence support the behavioral importance of this pathway in mammals (*67*, *68*). Our results, along with those of Lefton *et al.* (*66*), argue that the neuromodulatory effects of NE, and perhaps other neuromodulators, must be reconsidered under the lens of astroglial modulation of neurophysiology and circuit dynamics.

Feedforward inhibition is widespread in synaptically coupled circuits (*53*, *54*, *69*, *70*). Synaptic feedforward inhibition serves many functions, such as improving the spatial and

temporal precision of neural coding (*53*, *54*), gain control (*69*), and improving sensory acuity (*70*). Here, we show that feedforward inhibition can also be implemented through molecular circuits to play similar computational roles on much longer timescales (tens of seconds) that are complementary to the millisecond timescales of neuronal feedforward inhibition. Although astroglial activation by NE is widespread and quite synchronized, output diversification may occur at each step, from ATP release to ATP-to-adenosine metabolism and finally to adenosine receptor activation. For example, adenosine receptor expression could be altered in different brain regions, the sensitivity of astroglia to NE could be modulated by local neuronal activity, or the activity of the extracellular enzymes that transform ATP into adenosine could be tuned to modulate this extrasynaptic circuit motif in a context-dependent manner. Astroglia-mediated feedforward inhibition may therefore be similarly flexible and ubiquitous but operate on slower timescales.

Over the past few decades, several lines of work have raised the possibility of an evolutionarily conserved role for the NAP motif in feedforward inhibition. Classic work has shown that an ATP-to-adenosine pathway acts in the spinal cord to inhibit locomotion in tadpoles (*35*), and more recent work suggests that astroglia contribute to spinal cord ATP release and locomotion suppression in rodents (*71*). Astroglia have also been shown to drive the inhibitory phases of a variety of episodic behaviors such as sleep (*72*) and sensory-evoked arousal (*30*, *73*). We speculate that the seemingly conserved role for astroglia in feedforward inhibition after rapid excitation may reflect—and may have arisen from—a fundamental astroglial function to regulate neuronal network excitability. Indeed, both astroglia and purinergic signaling play central roles in controlling excitability (*64*, *74*), and astroglial and purinergic dysfunction is implicated in epileptic seizure generation (*75*). Because astroglia have multiple molecular pathways for modulating neuronal excitation, such as those involved in potassium buffering, purinergic release, and glutamate metabolism (*75*, *76*), an ancestral astroglial role in excitability regulation may have been appropriated to modulate circuit activity in many different behaviorally relevant contexts to modulate neuronal excitability.

REFERENCES AND NOTES

1. M. V. Bennett, Y. Nakajima, G. D. Pappas, *J. Neurophysiol.* **30**, 161–179 (1967).
2. A. Bhattacharya, U. Aghayeva, E. G. Berghoff, O. Hobert, *Cell* **176**, 1174–1189.e16 (2019).
3. S. J. Smith *et al.*, *eLife* **8**, e47889 (2019).
4. M. Lovett-Barron *et al.*, *Cell* **171**, 1411–1423.e17 (2017).
5. J. C. Marques, M. Li, D. Schaak, D. N. Robson, J. M. Li, *Nature* **577**, 239–243 (2020).
6. C. I. Bargmann, E. Marder, *Nat. Methods* **10**, 483–490 (2013).
7. F. Randi, A. K. Sharma, S. Dvali, A. M. Leifer, *Nature* **623**, 406–414 (2023).
8. L. Ripoll-Sánchez *et al.*, *Neuron* **111**, 3570–3589.e5 (2023).
9. S. L. Hooper, E. Marder, *Brain Res.* **305**, 186–191 (1984).
10. S. R. Yeh, R. A. Fricke, D. H. Edwards, *Science* **271**, 366–369 (1996).
11. P. S. Katz, P. A. Getting, W. N. Frost, *Nature* **367**, 729–731 (1994).
12. J. S. Coggan *et al.*, *Science* **309**, 446–451 (2005).
13. G. Mountoufaris *et al.*, *Cell* **187**, 5998–6015.e18 (2024).
14. J. Nagai *et al.*, *Neuron* **109**, 576–596 (2021).
15. E. A. Bushong, M. E. Martone, Y. Z. Jones, M. H. Ellisman, *J. Neurosci.* **22**, 183–192 (2002).
16. G. Perea, M. Navarrete, A. Araque, *Trends Neurosci.* **32**, 421–431 (2009).
17. U. S. V. Euler, *Nature* **156**, 18–19 (1945).
18. R. Jordan, *Trends Neurosci.* **47**, 92–105 (2024).
19. R. Jordan, G. B. Keller, *eLife* **12**, RP85111 (2023).
20. D. G. R. Tervo *et al.*, *Cell* **159**, 21–32 (2014).
21. S. J. Sara, S. Bouret, *Neuron* **76**, 130–141 (2012).
22. G. Aston-Jones, J. D. Cohen, *Annu. Rev. Neurosci.* **28**, 403–450 (2005).
23. M. E. Hasselmo, C. Linster, M. Patil, D. Ma, M. Cekic, *J. Neurophysiol.* **77**, 3326–3339 (1997).
24. V. Zerbi *et al.*, *Neuron* **103**, 702–718.e5 (2019).
25. E. Bülbring, J. H. Burn, *J. Physiol.* **101**, 289–303 (1942).
26. A. Uribe-Arias *et al.*, *Neuron* **111**, 4040–4057.e6 (2023).
27. L. K. Bekar, W. He, M. Nedergaard, *Cereb. Cortex* **18**, 2789–2795 (2008).
28. F. Ding *et al.*, *Cell Calcium* **54**, 387–394 (2013).
29. Z. Ma, T. Stork, D. E. Bergles, M. R. Freeman, *Nature* **539**, 428–432 (2016).
30. M. E. Reitman *et al.*, *Nat. Neurosci.* **26**, 579–593 (2023).
31. T. Porkka-Heiskanen *et al.*, *Science* **276**, 1265–1268 (1997).
32. W. Peng *et al.*, *Science* **369**, eabb0556 (2020).
33. A. Suppermpool, D. G. Lyons, E. Broom, J. Rihel, *Nature* **629**, 639–645 (2024).
34. O. Pascual *et al.*, *Science* **310**, 113–116 (2005).
35. N. Dale, D. Gilday, *Nature* **383**, 259–263 (1996).
36. M. Wall, N. Dale, *Curr. Neuropharmacol.* **6**, 329–337 (2008).
37. D. van Calker, K. Biber, K. Domschke, T. Serchov, *J. Neurochem.* **151**, 11–27 (2019).
38. L. Weltha, J. Reemmer, D. Boison, *Brain Res. Bull.* **151**, 46–54 (2019).
39. T. V. Dunwiddie, L. Diao, W. R. Proctor, *J. Neurosci.* **17**, 7673–7682 (1997).
40. R. de Ceglia *et al.*, *Nature* **622**, 120–129 (2023).
41. D. Lovatt *et al.*, *Proc. Natl. Acad. Sci. U.S.A.* **109**, 6265–6270 (2012).
42. L. Yang, Y. Qi, Y. Yang, *Cell Rep.* **11**, 798–807 (2015).
43. M. J. Broadhead, G. B. Miles, *Front. Cell. Neurosci.* **14**, 30 (2020).
44. G. R. J. Gordon *et al.*, *Nat. Neurosci.* **8**, 1078–1086 (2005).
45. M. B. Orger, M. C. Smear, S. M. Anstis, H. Baier, *Nat. Neurosci.* **3**, 1128–1133 (2000).
46. E. Yang *et al.*, *Cell* **185**, 5011–5027.e20 (2022).
47. N. Jurisch-Yaksi, E. Yaksi, C. Kizil, *Glia* **68**, 2451–2470 (2020).
48. J. Chen, K. E. Poskanzer, M. R. Freeman, K. R. Monk, *Nat. Neurosci.* **23**, 1297–1306 (2020).
49. Y. Mu *et al.*, *Cell* **178**, 27–43.e19 (2019).
50. M. Duque *et al.*, *Neuron* **113**, 426–443.e5 (2025).
51. L. Rinaman, *Am. J. Physiol. Regul. Integr. Comp. Physiol.* **300**, R222–R235 (2011).
52. G. Moruzzi, H. W. Magoun, *Electroencephalogr. Clin. Neurophysiol.* **1**, 455–473 (1949).
53. F. Pouille, M. Scanziani, *Science* **293**, 1159–1163 (2001).
54. W. Mittmann, U. Koch, M. Häusser, *J. Physiol.* **563**, 369–378 (2005).
55. A. V. Gourine *et al.*, *Science* **329**, 571–575 (2010).
56. T. A. Babola *et al.*, *J. Neurosci.* **41**, 594–612 (2021).
57. Z. Wu *et al.*, *Neuron* **110**, 770–782.e5 (2022).
58. W.-H. Cho, E. Barcelon, S. J. Lee, *Exp. Neurobiol.* **25**, 197–204 (2016).
59. E. Gerasimov *et al.*, *Int. J. Mol. Sci.* **22**, 9613 (2021).
60. S. A. Sloan, B. A. Barres, *Neuron* **84**, 1112–1115 (2014).
61. W. Boehmler *et al.*, *Gene Expr. Patterns* **9**, 144–151 (2009).
62. C. Li *et al.*, *Neuron* **111**, 2727–2741.e7 (2023).
63. M. Corkrum *et al.*, *Neuron* **105**, 1036–1047.e5 (2020).
64. S. Pittolo *et al.*, *Cell Rep.* **40**, 111426 (2022).
65. T. Deemyad, J. Lüthi, N. Spruston, *Nat. Commun.* **9**, 4336 (2018).
66. K. B. Lefton *et al.*, *Science* **388**, 776 (2025).
67. Q. Xin *et al.*, *Cell* 10.1016/j.cell.2025.04.010 (2025).
68. G. T. Drummond *et al.*, Cortical norepinephrine-astrocyte signaling critically mediates learned behavior. bioRxiv 620009 [Preprint] (2024); https://doi.org/10.1101/2024.10.24.620009
69. S. R. Olsen, R. I. Wilson, *Nature* **452**, 956–960 (2008).
70. M. Wehr, A. M. Zador, *Neuron* **47**, 437–445 (2005).
71. D. Acton, G. B. Miles, *PLOS ONE* **10**, e0134488 (2015).
72. M. M. Halassa *et al.*, *Neuron* **61**, 213–219 (2009).
73. J. Lines, E. D. Martin, P. Kofuji, J. Aguilar, A. Araque, *Nat. Commun.* **11**, 3689 (2020).
74. A. Badimon *et al.*, *Nature* **586**, 417–423 (2020).
75. C. Diaz Verdugo *et al.*, *Nat. Commun.* **10**, 3830 (2019).
76. T. Miyashita *et al.*, *Science* **382**, eadf7429 (2023).
77. Data and analysis code for: A. B. Chen *et al.*, Norepinephrine changes behavioral state through astroglial purinergic signaling, Zenodo (2025); https://doi.org/10.5281/zenodo.14278354

ACKNOWLEDGMENTS

We thank M. Ellisman, D. Bergles, Y. Mu, and L. Looger, as well as members of the Engert and Ahrens labs, for discussions and feedback. **Funding:** This work was supported by Boehringer Ingelheim Fonds (Graduate Fellowship to M.Du. and A.R.), the European Research Council (ERC Consolidator grant ERC-CoG-101002870 to C.W.), the European Union (Horizon 2020 Research and Innovation program Marie Skłodowska-Curie grant 813457 to C.W.), Fondation Bettencourt Schueller (grant FBS-don-0031 to C.W.), the Howard Hughes Medical Institute (A.B.C., M.Du., S.N., M.B.A.); the Janelia Research Campus (Graduate Research Fellowship to A.B.C. and Visiting Scientist Program positions for A.B.C., M.Du., and V.W.); the National Institutes of Health (grant R35NS122172 to D.A.P., grants U19NS104653 and 1R01NS124017 to F.E., and grants U19NS123719 and R01MH110504 to G.Y.), the National Science Foundation (grant IIS-1912293 to F.E. and grant GRFP DGE1745303 to A.B.C.), and the Simons Foundation (grant SCGB 542943SPI to F.E. and M.B.A.). **Author contributions:** Conceptualization: A.B.C., M.B.A.; Funding acquisition: G.Y., C.W., D.A.P., F.E., M.B.A.; Investigation: A.B.C., M.Du.; Methodology: A.B.C., M.Du., A.R., M.Dh., V.M.W., X.M., A.R., E.M.L., M.E., S.N., D.A.P., G.Y.; Project administration: A.B.C., F.E., M.B.A.; Supervision: G.Y., C.W., D.A.P., F.E., M.B.A.; Visualization: A.B.C., M.Du., X.M.; Writing – original draft: A.B.C., M.B.A.; Writing – review & editing: all authors. **Competing interests:** The authors declare no competing interests. **Data and materials availability:** Data and analysis code are available at Zenodo (*77*).

SUPPLEMENTARY MATERIALS

science.org/doi/10.1126/science.adq5233
Materials and Methods; Figs. S1 to S10; Table S1; References (*78*–*92*); MDAR Reproducibility Checklist; Movie S1

Submitted 20 May 2024; accepted 6 December 2024

10.1126/science.adq5233